

Suchomimus. The cervical series in both *Baryonyx* and *Suchomimus* shows a dorsal offset of the anterior articular surfaces.

19. E. Buffetaut, *Neues Jahrb. Geol. Palaeontol. Monh.* **1992**, 88 (1992).

20. C. W. Gilmore, *Bull. U.S. Natl. Mus.* **110**, 1 (1920).

21. P. C. Sereno et al., *Science* **272**, 986 (1996).

22. The following 45 synapomorphies (optimized with delayed transformation) correspond with the scored character states [(0) or (1)] (Table 2) that were used in the analysis of the spinosaurid relationships presented in Fig. 4A. Synapomorphies 27 through 34 uniting *Baryonyx* and *Suchomimus* cannot be observed in other spinosaurids because of incomplete preservation. **Spinosaurioidea**: 1, anterior ramus of maxilla, length: 70% (0) or 100% or more (1) of maximum depth; 2, lacrimal anterior ramus, length: more (0) or less (1) than 65% of the ventral ramus; 3, humeral deltopectoral crest, length: less (0) or more (1) than 45% of humeral length; 4, radial (forearm) length: more (0) or less (1) than 50% of humeral length; 5, manual digit I-ungual, length: 2.5 (0) or 3 (1) times the depth of the proximal end. **Spinosauridae**: 6, anterior end of upper and lower jaws, form: convergent (0); expanded into a premaxillary/dentary rosette (1); 7, snout length: less (0) or more (1) than three times the length of the antorbital fenestra; 8, external nares positioned entirely posterior to the premaxillary tooth row; 9, antorbital fossa, size: larger (0) or smaller (1) than the orbit; 10, interpremaxillary suture, form: open (0); fused (1) at maturity; 11, premaxillary-maxillary articulation, form: scarf or butt joint (0); interlocking (1); 12, maxillary anteromedial process, shape: fluted prong (0); plate (1); 13, maxillary antero-medial process, anterior extension: as far as (0) or far anterior to (1) the anterior margin of the maxilla; 14, parodontal laminae: present (0); absent (1); 15, lacrimal anterior and ventral rami, angle of divergence: 75° to 90° (0); 30° to 45° (1); 16, splenial foramen, size: small (0); large (1); 17, midcrown cross section: elliptical (0); circular (1); 18, crown striations: absent (0); present (1); 19, premaxillary tooth count: 3 to 4 (0); 6 to 7 (1); 20, maxillary crowns, spacing: adjacent (0); with intervening space (1); 21, distal root shape: broad (0); strongly tapered (1). **Baryonychinae (Suchomimus and Baryonyx)**: 22, anterior dorsal centra, depth of ventral keel: weak (0); blade-shaped (1); 23, maximum height of dorsal neural spines: less (0) or more (1) than 2.5 times the centrum height; 24, posterior dorsal neural spines, basal webbing: absent (0); present (1); 25, posterior dorsal neural spines, accessory centrodiapophyseal lamina: absent (0); present (1); 26, dentary tooth count: ~15 (0); ~30 (1); 27, quadrate head, shape: oval (0); subquadrate (1); 28, quadrate foramen, size: foramen (0); broad fenestra (1); 29, coracoid posterior process, shape: low and rounded (0); crescentic (1); 30, humeral trochanters, size: low and rounded (0); hypertrophied (1); 31, humeral deltopectoral crest, orientation of apex: anterior (0); lateral (1); 32, humeral internal tuberosity, size: low and rounded (0); hypertrophied (1); 33, radial external tuberosity and ulnar internal tuberosity, size: low and rounded (0); hypertrophied (1); 34, pubic foot, size: moderate to large (0); reduced to a small flange (1). **Spinosaurinae (Irritator and Spinosaurus)**: 35, crown recurvature: present (0); very reduced or absent (1); 36, crown serrations: present (0); absent (1). 37, dentary crowns, spacing: adjacent (0); with intervening space (1); 38, premaxillary tooth 1, size: slightly smaller (0) or much smaller (1) than crowns 2 and 3; 39, diastemata within the premaxillary rosette: narrow (0); broad (1). **Torvosauridae**: 40, antorbital fossa, width of ventral margin: more (0) or less (1) than 30% of the maximum depth of the posterior (principal) ramus; 41, subcircular depression in the anterior corner of the antorbital fossa: absent (0); present (1); 42, lacrimal foramen, position: near the base (0) or at midheight (1) on the ventral process; 43, jugal posterior ramus, depth: less (0) or more (1) than that of the orbital ramus; 44, postorbital ventral process, cross section of distal half: subcircular (0); U-shaped (1); 45, puboischial fenestra: broadly open (0); closed or nearly closed (1).

23. F. von Huene, *Rev. Mus. La Plata* **29**, 35 (1926); S.-Y. Hu, *Vertebr. Palasiat.* **8**, 42 (1964); P. M. Galton and J. A. Jensen, *BYU Geol. Stud.* **26**, 1 (1979); J. A. Jensen, *Great Basin Nat.* **45**, 710 (1985); B. B. Britt, *BYU Geol. Stud.* **37**, 1 (1991).

24. A previous cladistic analysis placed spinosaurids as the sister taxon to Neotetanurae (13). Notably, synapomorphies linking spinosaurids and torvosaurids were simply ignored in that analysis, and spinosaurids and neotetanurans were joined by one character with an ambiguous optimization (a hook-shaped coracoid).

25. The expanded terminal rosette has a very specific structure in spinosaurids that is probably related to the manner in which its teeth articulate. Seven premaxillary teeth are opposed by five dentary teeth. Three diastemata are present in the upper rosette (between teeth 3 and 4, between teeth 5 and 6, and between tooth 7 and the maxillary teeth).

26. Baryonychinae (11) is defined here as all spinosaurids that are more closely related to *Baryonyx* than to *Spinosaurus*; this clade currently includes *Baryonyx* and *Suchomimus*. Spinosaurinae (1) is defined here as all spinosaurids that are more closely related to *Spinosaurus* than to *Baryonyx*; this clade currently includes *Spinosaurus* and *Irritator* (= *Angaturama*).

27. Revised diagnosis for *Baryonyx walkeri*: Spinosaurid characterized by fused nasals with a median crest terminating posteriorly in a cruciate process, a solid subrectangular lacrimal horn, a marked transverse constriction of the sacral or anterior caudal centra, a well-formed peg-and-notch articulation between the scapula and coracoid, an everted distal margin of the pubic blade, and a very shallow fibular fossa.

28. Biogeographic hypotheses were optimized with dispersal-vicariance analysis [F. Ronquist, *Syst. Biol.* **46**, 195 (1997)], which counts the minimum number of dispersal or extinction events that is required to account for the observed distributions. There is no

cost associated with vicariance. In our example, there is only one hypothesis that requires a single event (dispersal from Europe to Africa during the Early Cretaceous), if one accepts the general pattern of continental breakup as described in the text.

29. E. Buffetaut, *Terra Nova* **1**, 69 (1989); J. Le Loeuff, *Cretaceous Res.* **12**, 93 (1991).

30. E. Stromer, *Abh. Bayer. Akad. Wiss. Math. Naturwiss. Abt. N. F.* **22**, 1 (1934).

31. A. G. Smith, D. G. Smith, B. M. Funnell, *Atlas of Mesozoic and Cenozoic Coastlines* (Cambridge Univ. Press, Cambridge, 1994), p. 41.

32. D. L. Swofford, PAUP 3.1 (Illinois Natural History Survey, Champaign, IL, 1993).

33. W. B. Harland et al., *A Geologic Time Scale* (Cambridge Univ. Press, Cambridge, 1989).

34. Supported by the David and Lucile Packard Foundation, National Geographic Society, Pritzker Foundation, and the Women's Board of the University of Chicago. We thank K. Bainbridge, A. Boldizar, J. Bradshaw, J.-P. Cavignelli, J. Ogradnick, and F. Stroik for participation in field excavation; C. Abraczinskas for drawing from the original specimens and executing the final drafts of Figs. 1A and 2 through 4; B. Strack (Field Museum) for assistance with microphotography; Q. Cao and E. Dong for directing fossil preparation and casting; and J. Hopson, F. Lando, R. Molnar, and H.-D. Sues for reviewing an earlier draft of the paper. We gratefully acknowledge the assistance of I. Kouada of the Ministère de l'Enseignement Supérieur de la Recherche et de la Technologie (Niger). For permission to conduct fieldwork, we are indebted to the Republic of Niger.

31 August 1998; accepted 2 October 1998

Ultrastable Mesostructured Silica Vesicles

Seong Su Kim, Wenzhong Zhang, Thomas J. Pinnavaia*

A family of mesoporous molecular sieves (denoted MSU-G) with vesicle-like hierarchical structures and unprecedented thermal (1000°C) and hydrothermal stabilities (more than 150 hours at 100°C) associated with high SiO₄ cross-linking was prepared through a supramolecular assembly pathway that relies on hydrogen bonding between electrically neutral gemini surfactants of the type C_nH_{2n+1}NH(CH₂)₂NH₂ and silica precursors derived from tetraethylorthosilicate. The vesicle shells are constructed of one or more undulated silica sheets that are about 3 nanometers thick with mesopores (average diameters from 2.7 to 4.0 nanometers) running both parallel and orthogonal to the silica sheets, which makes the framework structure bicontinuous and highly accessible. Catalytic metal ion centers [for example, Ti(IV) and Al(III)] have been incorporated into the framework with the retention of hierarchical structure.

Substantial progress has been made recently in extending the supramolecular assembly of mesostructured inorganic framework structures to include hierarchical forms with a variety of particle shapes (1-3). Mesoporous metal oxide molecular sieves with vesicle-like morphologies are of interest as potential catalysts and sorbents, in part because the mesostructured shells and intrinsic textural pores of the vesicles should efficiently transport guest species to framework binding sites. However, all vesicle-

like mesostructures reported to date had shells of undesirable thickness. More important, like many mesoporous molecular sieves with conventional particle morphologies, the framework structures defining the vesicle shells were lacking in structural stability. For instance, a vesicular aluminophosphate with mesoscale *d* spacing and surface patterns that mimicked diatom and radiolarian skeletons collapsed to AlPO₄-cristobalite with a complete loss of the hierarchical patterns at 300°C (4). Also, vesicle-like silicic acid polymers that were structured by a didodecyltrimethylammonium bromide template lost their hierarchical structures when washed with alcohols (5). Macroscopic hollow spheres of mesoporous MCM-41 (2, 6) have been prepared from oil-in-water emulsions, but

Department of Chemistry and Center for Fundamental Materials Research, Michigan State University, East Lansing, MI 48824, USA.

*To whom correspondence should be addressed. E-mail: Pinnavaia@cem.msu.edu

these particles had shells that were very thick (1000 to 5000 nm) and were comparable in size to mesostructured particles with conventional shapes. The feasibility of forming vesicular mesoporous silicas has been demonstrated recently by an assembly pathway based on the use of an amine bolaamphiphile as the structure-directing agent (7). However, the shell thickness (100 to 250 nm) was large in comparison to the vesicle diameter (300 to 800 nm). More important, the thermal and hydrothermal stability was unremarkable, and the particle shape deviated greatly from the desired vesicular form with increasing surfactant chain length (8). Here we report a direct and highly efficient synthesis route to an entire family of vesicular mesoporous silicas (denoted MSU-G) with very thin shells (~3 to 70 nm) and diameters of 20 to 1400 nm. Moreover, the degree of framework SiO_4 unit cross-linking is unprecedented among mesoporous silicas, making these materials ultrastable in relation to previously reported mesostructures.

Certain lamellar phospholipid phases (9) and related L_α bilayer surfactant phases (10) are attractive candidates for the incorporation of vesicle-like hierarchical features into a silica mesostructure because these phases readily form vesicles in an aqueous solution. A surfactant L_α liquid crystal phase can undergo concentration- and temperature-dependent transitions to a bicontinuous wormhole or to sponge-like L_3 phases (11) (Fig. 1A). The L_α -to- L_3 transition proceeds through an intermediate that links the undulated bilayers through elementary passages. Our goal was to assemble lamellar silica mesostructures with single or connected lamellae in a manner analogous to the bicontinuous L_α - L_3 intermediate, while minimizing the surface energy through vesicle formation. To achieve a vesicular silica with a framework analogous to the L_α - L_3 intermediate structure, we also needed to avoid the formation of a thermodynamically favored L_3 sponge-like phase. L_3 silicate mesophases formed from liquid crystal templates were investigated by McGrath *et al.* (12) and were not found to form vesicles.

Although several surfactant systems are known to direct the assembly of lamellar silica mesostructures (7, 8, 13, 14), none are capable of generating an entire family of stable mesoporous silicas with vesicular particle forms. We have found, however, that an electrically neutral hydrogen-bonding pathway based on the hydrolysis of tetraethylorthosilicate (TEOS) in the presence of gemini surfactants of the type $\text{C}_n\text{H}_{2n+1}\text{NH}(\text{CH}_2)_2\text{NH}_2$ (15) (abbreviated as C°_{n-2-0}) exhibits the thermodynamic structure-directing ability and kinetic lability needed to form silica mesostructures that are analogous to the L_α - L_3 intermediate in almost-quantitative yield. In contrast to the cationic quaternary ammonium ion forms of gemini surfactants, which effectively direct the electrostatic assembly of three-dimensional (3D) silica mesostruc-

tures with conventional particle morphologies (16), our electrically neutral gemini derivatives provide vesicular hierarchical structures.

As illustrated schematically in Fig. 1B, MSU-G silicas were obtained by the cooperative transformation of TEOS and a lamellar C°_{n-2-0} phase into an undulated lamellar mesostructure under hydrothermal reaction conditions (17). The x-ray diffraction (XRD) pattern of the initial surfactant solution in the absence of TEOS (Fig. 1C) reveals the presence of two lamellar phases with basal spacings (3.56 and 3.29 nm) that differ by one water layer between lipidlike bilayers. These two phases were also observed in a thin-film sample of the surfactant supported on glass. The surfactant-containing MSU-G mesostructures and the surfactant-free forms obtained by calcination at 650°C and 1000°C exhibit one or, at most, two diffraction lines (Fig. 1D) that are consistent with an undulated lamellar structure analogous to the surfactant intermediate encountered in an L_α - L_3 surfactant transformation (compare Fig. 1A).

A representative transmission electron microscope (TEM) image illustrates the vesicular morphology of MSU-G silicas (Fig. 2A). Three C°_{n-2-0} surfactants ($n = 10, 12,$ and 14) form silica mesostructures with the same dominant vesicle-like shapes. Almost all of the particles (>90%) may be described as being complete vesicles or, more commonly, ruptured vesicles (Fig. 2, B and C) and bowls (Fig. 2D). The rims of the bowls and the edges of the ruptured vesicles clearly reveal a framework structure made of undulated silica layers ~3.0 nm thick with irregularly spaced mesopores running parallel to the lamellae. Bridging of the silica layers is also evident in the micrographs, further verifying the structural relation to the intermediate formed in an L_α - L_3 surfactant phase transition (compare Fig. 1A). In addition, the rounded surfaces of the vesicular and bowl-shaped fragments show randomly distributed framework pores orthogonal to the silica sheets. Thus, each 3-nm-thick sheet contains mesopores that connect to the interlayer mesopores,

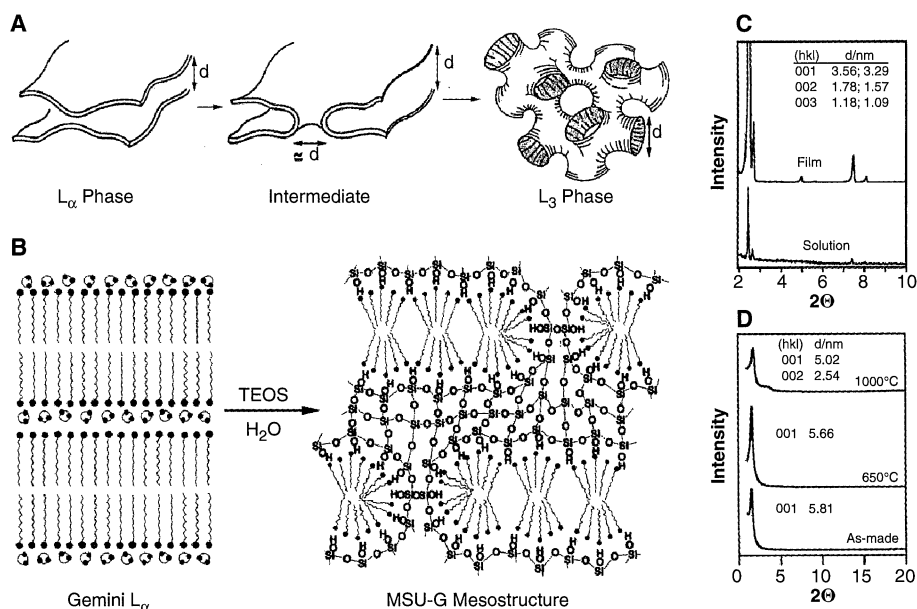


Fig. 1. (A) Schematic representation of a surfactant L_α -to- L_3 phase transition showing an intermediate in which adjacent bilayers are connected through an elementary passage (17). (B) The pathway used for the preparation of mesostructured MSU-G silicas. (C) The XRD patterns for the pristine surfactant were recorded for a 88:12 (v/v) water:ethanol suspension of neutral C°_{12-2-0} gemini surfactant at the same concentration (3.0 weight %) used for MSU-G synthesis (16) and a thin-film sample of the surfactant on glass. (D) The XRD pattern for the surfactant-containing and calcined MSU-G samples. The patterns were obtained on a Rigaku Rotaflex diffractometer that was equipped with a rotating anode and $\text{Cu } K_\alpha$ radiation (wavelength = 0.1542 nm).

Table 1. Pore sizes, basal spacings, FWT, and BET surface areas (S_{BET}) of mesoporous MSU-G silicas calcined at 650°C and the Q^4/Q^3 ratios for the framework SiO_4 units in the surfactant-containing mesostructures. The FWT was determined by the difference between the d spacing and the HK pore size.

Gemini surfactant	Pore size (nm)	d spacing (nm)	FWT (nm)	S_{BET} (m^2/g)	Q^4/Q^3
C°_{10-2-0}	2.7	4.80	2.1	523	7.1
C°_{12-2-0}	3.2	5.66	2.5	412	6.2
C°_{14-2-0}	4.0	6.49	2.5	279	7.4

REPORTS

creating the 3D pore system. Consistent with vesicle formation through a layer propagation and bending process, the smaller vesicles with diameters in the range from ~ 20 to 125 nm have very thin unilamellar shells (~ 3 nm), whereas the larger vesicles with diameters up to 1400 nm have multilamellar shells up to ~ 70 nm in thickness.

The N_2 adsorption-desorption isotherms and the Horvath-Kawazoe (HK) pore size distributions for calcined MSU-G silicas that were prepared from gemini surfactants of differing alkyl chain length are shown in Fig. 3. The adsorption steps at relative pressures between 0.20 and 0.65 signify the filling of framework mesopores, and the hysteresis loops at higher relative pressures are a consequence of N_2 filling the textural mesopores that are associated with a vesicular (lamellar) particle morphology. In accord with an assembly pathway based on hydrogen bond interactions between the surfactant and the inorganic framework walls, the surfactant could be readily removed from the framework pores by hot ethanol extraction, as shown by ^{13}C cross-polarized magic angle

spinning (MAS) nuclear magnetic resonance (NMR). The N_2 adsorption and desorption isotherms for the solvent-extracted samples were almost identical to those obtained for the calcined derivative.

The maxima in the HK pore size distribution curves increase 2.7, 3.2, and 4.0 nm as the surfactant chain length is increased over the range $n = 10, 12,$ and 14 , respectively (Table 1). Also, an increase in the surfactant chain length increases both the d spacing and the pore size. Thus, the framework wall thickness (FWT) remains almost constant (2.1 to 2.5 nm) and in reasonable agreement with the value estimated from TEM images (~ 3.0 nm). The FWT values are ~ 2.5 to 3.0 times greater than the values observed for electrostatically assembled MCM-41 silicas (18, 19). Accordingly, the thicker framework walls result in Brunauer-Emmett-Teller (BET) surface areas (280 to 520 m^2/g) that are proportionately lower than the values typically found for MCM-41 (900 to 1200 m^2/g).

Another important distinction between MSU-G silicas and previously reported meso-

porous silicas is the very high degree of SiO_4 unit cross-linking in the framework and the structural stability that results from this cross-linking. As shown by the deconvoluted ^{29}Si MAS NMR spectra in Fig. 4, the surfactant-containing MSU-G framework consists primarily of fully cross-linked Q^4 (SiO_4 units, with the exponent specifying the number of oxygen atoms that is corner-shared with adjacent SiO_4 units) unit [with a resonance near -110 parts per million (ppm) and a smaller fraction of incompletely cross-linked Q^3 sites (-98 ppm)]. Three different surfactant-containing MSU-G mesostructures yielded Q^4/Q^3 ratios in the range from 6.2 to 7.4 (compare Table 1). Normally, surfactant-containing silica mesostructures, whether assembled from ionic or neutral surfactants, exhibit Q^4/Q^3 ratios that are less than 2.0, and their calcined derivatives typically have values near 3.0 (13, 19). The Q^4/Q^3 ratios for MSU-G do not change greatly upon calcination at $650^\circ C$, suggesting that the $SiOH$ groups may be site isolated and buried in the framework.

Consistent with the remarkable degree of

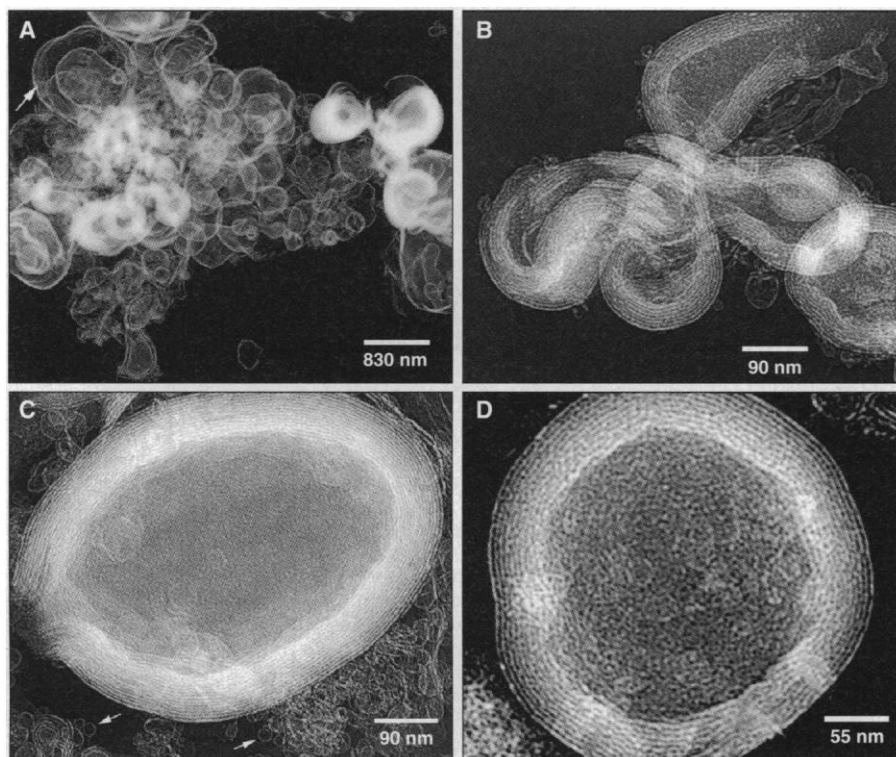


Fig. 2. TEM images of calcined ($650^\circ C$) hierarchical forms of MSU-G silica assembled from a $C_{12}H_{25}NH(CH_2)_2NH_2$ gemini surfactant. (A) The dominant vesicular morphology. The arrow points to one of the largest vesicles (diameter, ~ 1400 nm; shell thickness, ~ 40 nm). (B) Fractured multilamellar vesicles and bowls. Wormholelike framework mesopores are contained between the undulated silica sheets of the multilamellar vesicles. Each silica layer is ~ 3 nm thick. (C) and (D) The presence of wormholelike framework pores that run orthogonal to the undulated silica sheets, creating the 3D pore network. The arrows in (C) point to unilamellar vesicles that are ~ 20 nm in diameter. The same hierarchical forms were observed in silicas assembled from gemini surfactants containing alkyl chains with 10 and 14 carbon atoms. The micrographs were obtained on a JEOL 100CX instrument with an electron beam generated by a CeB_6 gun that was operating at an acceleration voltage of 120 kV. The specimens were loaded onto a holey carbon film that was supported on a copper grid by dipping the grid in a suspension of MSU-G (1 weight %) in ethanol.

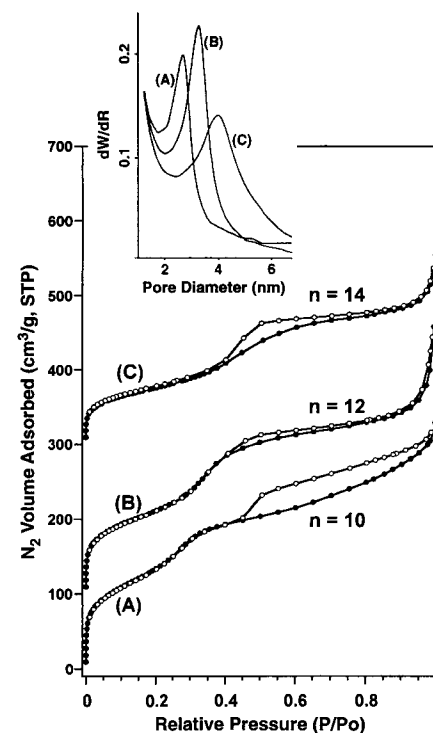


Fig. 3. N_2 adsorption-desorption isotherms for calcined ($650^\circ C$) MSU-G silicas that were assembled from $C_nH_{2n+1}NH(CH_2)_2NH_2$ surfactants. The inset provides the HK pore size distributions that were obtained from the adsorption branch of the isotherms. The isotherms were measured by a Micromeritics ASAP 2010 sorptometer at $-196^\circ C$. Samples were out-gassed at $150^\circ C$ overnight under vacuum (10^{-5} torr). Isotherms B and C have been offset by 100 and 300 cm^3/g , respectively, along the vertical axis for clarity. STP, standard temperature and pressure; dW , derivative of the gas volume adsorbed; dR , derivative of the pore diameter.

framework cross-linking, the thermal and hydrothermal stabilities of MSU-G silicas are unprecedented among all previously reported mesostructures, regardless of framework composition or structure. In addition to being structurally stable during calcination at 1000°C (compare Fig. 1B), MSU-G silicas are stable in boiling water for >150 hours. In contrast, we find that MCM-41 and other electrostatically assembled silicas with benchmarked hydrothermal stabilities [including framework-stabilized KIT-1 silica mesostructures (20) and the thick-walled SBA-15 family of silicas (21)] become x-ray amorphous and lose accessible framework mesoporosity in <50 hours when subjected to equivalent calcination and boiling.

The combination of a 3D pore network and a vesicle-like morphology, in addition to the remarkable thermal and hydrothermal stability, has important implications for the use of MSU-G silicas in chemical catalysis and molecular separations. Most mesostructured molecular sieves (particularly those prepared through an electrostatic pathway) exhibit framework pore lengths on a micrometer length scale, which is comparable to the length scale of the mesostructured particles themselves. Access to the framework sites can be limited by diffusion along the pore length, particularly in reactions in condensed media. A combined vesicular morphology and 3D pore network allow the average diameter and length of the mesopores within a particle to be more comparable in their dimensions, thus facilitating access. As a first step toward the catalytic applications of such structures, we have incorporated re-

dox-active Ti(IV) and acidic Al(III) centers into the framework of MSU-G silicas (through postsynthesis reactions with titanium isopropoxide and sodium aluminate) without altering the lamellar framework or the vesicular hierarchical structure.

References and Notes

- G. A. Ozin, *Acc. Chem. Res.* **30**, 17 (1997); H. Yang, N. Coombs, G. A. Ozin, *Nature* **386**, 692 (1997); S. Mann *et al.*, *Chem. Mater.* **9**, 2300 (1997).
- S. Schacht, Q. Huo, I. G. Voigt-Martin, G. D. Stucky, F. Schüth, *Science* **273**, 768 (1996).
- H.-P. Lin and C.-Y. Mou, *ibid.*, p. 765.
- S. Oliver, A. Kuperman, N. Coombs, A. Lough, G. A. Ozin, *Nature* **378**, 47 (1995).
- M. Dubois, T. Gulik-Krzywicki, B. Cabane, *Langmuir* **9**, 673 (1993).
- Q. Huo, J. Feng, F. Schüth, G. D. Stucky, *Chem. Mater.* **9**, 14 (1997).
- P. T. Tanev and T. J. Pinnavaia, *Science* **271**, 1267 (1996).
- P. T. Tanev, Y. Liang, T. J. Pinnavaia, *J. Am. Chem. Soc.* **119**, 8616 (1997).
- A. D. Bangham, M. M. Standish, J. C. Watkins, *J. Mol. Biol.* **13**, 238 (1965); G. Sessa and G. Weissmann, *J. Lipid Res.* **9**, 310 (1968).
- F. Auguste, J.-P. Douliéz, A.-M. Bellocq, E. J. Dufourc, *Langmuir* **13**, 666 (1997); J. Oberdisse, O. Regev, G. Porte, *J. Phys. Chem. B* **102**, 1102 (1998); M. Dubois and T. Zemb, *Langmuir* **7**, 1352 (1991); K. L. Herrington, E. W. Kaler, D. D. Miller, J. A. Zasadzinski, S. Chiruvolu, *J. Phys. Chem.* **97**, 13792 (1993); H. Hoffmann, C. Thunig, U. Munkert, H. W. Meyer, W. Richter, *Langmuir* **8**, 2629 (1992).
- G. Porte, *J. Phys. Cond. Matter* **4**, 8649 (1992).
- K. M. McGrath, D. M. Dabbs, N. Yao, I. A. Aksay, S. M. Gruner, *Science* **277**, 552 (1997).
- C. T. Kresge, M. E. Leonowicz, W. J. Roth, J. C. Vartuli, J. S. Beck, *Nature* **359**, 710 (1992); J. S. Beck *et al.*, *J. Am. Chem. Soc.* **114**, 10834 (1992).
- M. Ogawa, *J. Am. Chem. Soc.* **116**, 7941 (1994); Y. Lu *et al.*, *Nature* **389**, 364 (1997).
- F. Linsker and R. L. Evans, *J. Am. Chem. Soc.* **67**, 1581 (1945).
- Q. Huo, R. Leon, P. M. Petroff, G. D. Stucky, *Science* **268**, 1324 (1995).
- MSU-G mesostructures were prepared by the hydrolysis and polymerization of TEOS in a 1:9 (v/v) ethanol:water solution of a neutral $C_{n-2,0}$ gemini surfactant under hydrothermal conditions. The molar ratio of each reaction mixture was 1.0 TEOS:0.25 surfactant:4.3 ethyl alcohol:78 H₂O. TEOS was added to the surfactant in the water:ethanol-mixed solvent under rapid stirring for 30 min, and then the mixture was heated at 100°C in an autoclave for 48 hours under static condition. The product was filtered, washed with cold ethanol, and air-dried. Finally, the surfactant was removed from the surfactant-containing product by calcination in air at 650°C for 4 hours or by extraction with hot ethanol.
- V. Alfredsson *et al.*, *J. Chem. Soc. Chem. Commun.* **1994**, 921 (1994).
- P. T. Tanev and T. J. Pinnavaia, *Chem. Mater.* **8**, 2068 (1996).
- R. Ryoo, J. M. Kim, C. H. Shin, J. Y. Lee, *Stud. Surf. Sci. Catal.* **105**, 45 (1997); R. Ryoo *et al.*, *J. Phys. Chem.* **100**, 17718 (1996).
- D. Zhao *et al.*, *Science* **279**, 548 (1998).
- This research was supported by NSF through Chemistry Research Group grant CHE-9633798.

3 August 1998; accepted 13 October 1998.

Large-Scale Nitrogen Oxide Plumes in the Tropopause Region and Implications for Ozone

Dominik Brunner, Johannes Staehelin,* Dominique Jeker

Continuous measurements of nitrogen oxide and ozone were performed from a commercial airliner during 1 year at cruising altitudes below and above the tropopause. The upper tropospheric nitrogen oxides distribution was found to be strongly influenced by large-scale plumes extending about 100 to 1300 kilometers along the flight track. The plumes were frequently observed downwind of thunderstorms and frontal systems, which most probably caused upward transport of polluted air from the continental boundary layer or nitrogen oxide production in lightning strokes, or both. Particularly in summer, average ozone concentrations in the plumes were enhanced compared to the tropospheric background levels.

Nitrogen oxides ($NO_x = NO + NO_2$) in the tropopause region are important in the context of climate forcing, because NO_x is an important factor in photochemical ozone

formation (1) and controls the partitioning between OH and HO_2 radicals (2). Ozone is an efficient greenhouse gas in the upper troposphere (3), and oxidation by hydroxyl radicals (OH) regulates the lifetime of several radiatively and chemically active gases in the atmosphere. The increase in tropospheric O_3 resulting from growing anthropogenic emissions of NO_x and other O_3 precursors is believed to have substantially contributed to climate forcing, mostly in the second half of this century (amounting

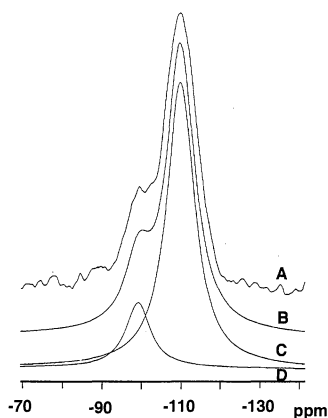


Fig. 4. Curve A is the experimental ^{29}Si MAS NMR spectrum of surfactant-containing MSU-G silica with the gemini surfactant $C_{12}H_{25}NH(CH_2)_2NH_2$ as the structure director. Curve (B) is the sum of the deconvoluted Q^4 (curve C) and Q^3 (curve D) spectral components with relative integral intensities of 6.2:1.0. The single-pulse mode ^{29}Si MAS NMR spectrum was recorded on a Varian VXR-400S spectrometer with a 7-mm zirconia rotor, a spinning frequency of 4 kHz, and a pulse delay of 800 s.

D. Brunner, Atmospheric Composition Research Division, Royal Netherlands Meteorological Institute, 3730 AE De Bilt, Netherlands. J. Staehelin and D. Jeker, Institute for Atmospheric Science, Swiss Federal Institute of Technology, ETH Hoenggerberg HPP, CH-8093 Zurich, Switzerland.

*To whom correspondence should be addressed. E-mail: staehelin@atmos.unm.ethz.ch